



Refractive Index Sensing Using Metamaterial Absorbing Augmentation in Elliptical Graphene Arrays

S. Dhanasekar¹ · K. Martin Sagayam² · Binay Kumar Pandey³ · Digvijay Pandey⁴

Received: 31 October 2023 / Accepted: 27 November 2023

© The Author(s), under exclusive licence to Springer Science+Business Media, LLC, part of Springer Nature 2023

Abstract

This research article proposes a periodically elliptical graphene metamaterial array-based wavelength-tunable absorber. The recent identification of graphene represents a substantial advancement in the field of plasmon-based electronics, which includes design, fabrication, wave distribution, inherent adaptability, and affordable prototyping. The finite difference time domain (FDTD) method is used to study the effects of different parameters. This article shows an apparent absorption peak with maximum absorption of 49.6% occurs at 55.12 μm compared to the existing metamaterial absorber. By extending the ellipse's major axis, increasing the X polarization of the incidence angle within a specific range, and enhancing graphene's chemical potential, the absorption rate of elliptical graphene arrays will be increased. Furthermore, to accurately evaluate the sensing capabilities of the structure, we model the spectra under varying refractive indexes in the environment, resulting in a design with a sensitivity (S) of up to 15,169 nm/RIU and a figure of merit (FOM) value. This research makes it easier to design environmental monitors, biosensors, and optoelectronic devices based on graphene.

Keywords Absorption enhancement · Metamaterial absorber · Graphene · Surface plasmon resonance · Finite difference time domain

Introduction

A periodic array of unit cells is formed to produce metamaterials, a particular class of artificial electromagnetic structure. They typically consist of fundamental electric

and magnetic resonance units, which allow electromagnetic waves with particular bands to exhibit resonance effects [1, 2]. It has always been exciting to explore the field of electromagnetic. THz electromagnetic radiation mainly lies within the infrared to microwave spectrum and has recently been used much more [3]. Thus, THz region devices are employed for various applications, including detecting and monitoring, sensing and switching, imaging, spectroscopy, and characterization [4]. Metals, graphene, and dielectrics can all be used to create metamaterials. The design and development of metamaterial perfect absorbers (MPA) has made use of the unique and distinctive characteristics of metamaterials, which include their negative refractive index (RI) [5]. Carbon atoms and sp² hybrid orbitals build up the hexagonal honeycomb structure of the two-dimensional (2D) carbon nanomaterial known as graphene [6]. It is possible to change the material's surface conductivity by providing a bias voltage or chemically doping graphene to vary the concentration of its carriers. Thus, dynamic modulation is possible with graphene [7]. Most engineering disciplines will be affected by digitalization, with rapid transfer of data wide-area networks for communication having the most significant effects [8–10]. The figure of merit is a numeric parameter used to

✉ Binay Kumar Pandey
binaydece@gmail.com

S. Dhanasekar
dhanasekar.sm@gmail.com

K. Martin Sagayam
martinsagayam.k@gmail.com

Digvijay Pandey
digit11011989@gmail.com

¹ Department of ECE, Sri Eshwar College of Engineering, Coimbatore 641202, India

² Department of ECE, Karunya Institute of Technology and Sciences, Coimbatore 641114, India

³ Department of Information Technology, College of Technology, Govind Ballabh Pant University of Agriculture and Technology, Pantnagar, Uttarakhand, India

⁴ Department of Technical Education (Government of Uttar Pradesh), Kanpur, India

compare the effectiveness of analytical methods based on their predictive abilities and their detection abilities. Sensitivity is usually determined by calibrating the sensor, which involves exposing it to known pressure levels and measuring the output.

Highly doped graphene is one of the most exciting materials because it can develop into a plasmonic material with incredible properties. Graphene has gained widespread usage in sensor applications, where adjustments to the Fermi level can readily influence the resonance wavelength spectrum. This attribute dramatically facilitates the achievement of a broad spectrum of sensing capabilities using graphene [11]. A design for a miniature C-shaped antenna using an artificial transmission line was proposed [12].

Plasmons are now often used in nonlinear optics, photoelectric device reconstruction, illness treatment, and single molecule-level hypersensitivity detection. In photodetectors and photovoltaic systems, graphene plasmons are essential [13]. The simulation for a fuzzy logic identification system utilizing a gravitational search algorithm has been discussed by Jubair et al. [14]. Recently, it was demonstrated that utilizing surface plasmon resonance, also known as SPR, for graphene using methods like strips [15], rings [16], crosses [18], and others, patterned graphene arrays will improve their absorption of incident energy. Xiao et al. [17] suggested the periodic ring graphene arrays in which acceptable angular polarization resulted in 25% absorption. Fang et al. [19] used a nanodisk graphene arrays for active devices to achieve a 30% absorption. On elliptical graphene arrays, however, more research needs to be done. The proposed structure can absorb 49.2% of the graphene material, known as a graphene-based absorber (GBA). It comprises arrays with periodic graphene elliptical metamaterial that are periodically patterned. Graphene's maximum absorption is restricted to 50% in a symmetrical environment [20].

This article presents a study of elliptical graphene-based optical absorption enhancement. If we add a golden mirror coating to the substrate, our proposed structure could achieve perfect absorption. An elliptical graphene-coated silica layer is added to the silicon foundation. Consequently, the proposed graphene-based absorber, with the highest absorption of 49.6%, remains an incredible result. The FOM and S associated with in the sensor-based design structure, which measures changes in surrounding refractive index, were 3.6 and 15,169 nm/RIU, respectively. Thus, tunable spectral detectors and sensors can be implemented using the elliptical array structure.

Geometric Structure of Elliptical Graphene Array Model

The production of expansive graphene sheets on gold surfaces has the potential to drive novel applications, particularly in spectroscopy and electrochemistry. Graphene can concentrate an enormous amount of light energy. Due to many good qualities of graphene, which have been arranged elliptically across the structure, can compensate for the metal's defects. The elliptical array of graphene is beneficial for light energy absorption. The catalytic activity of gold nanoparticles in oxidizing alcohols and carbon monoxide remains diameter-dependent. The gold nanoparticle created by the chemical vapor deposition (CVD) process can potentially understand when the graphene sheets on the gold surface evolve. The extraction procedures on deposition, gold foils as well as transfer procedure for graphene layers over dielectric substrates are schematically represented in Fig. 1 [21].

Highly pure gold plates pressed into gold foils approximately 25 m thick. The gold foils are cleaned of contaminants and then annealed with hydrogen flames for 20 min

Fig. 1 Graphene growth process, transfer, and deposition over gold film

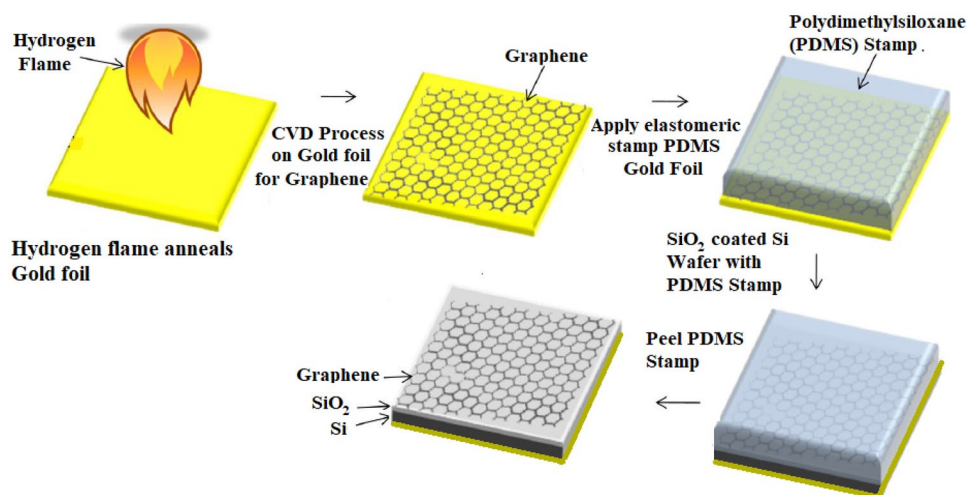
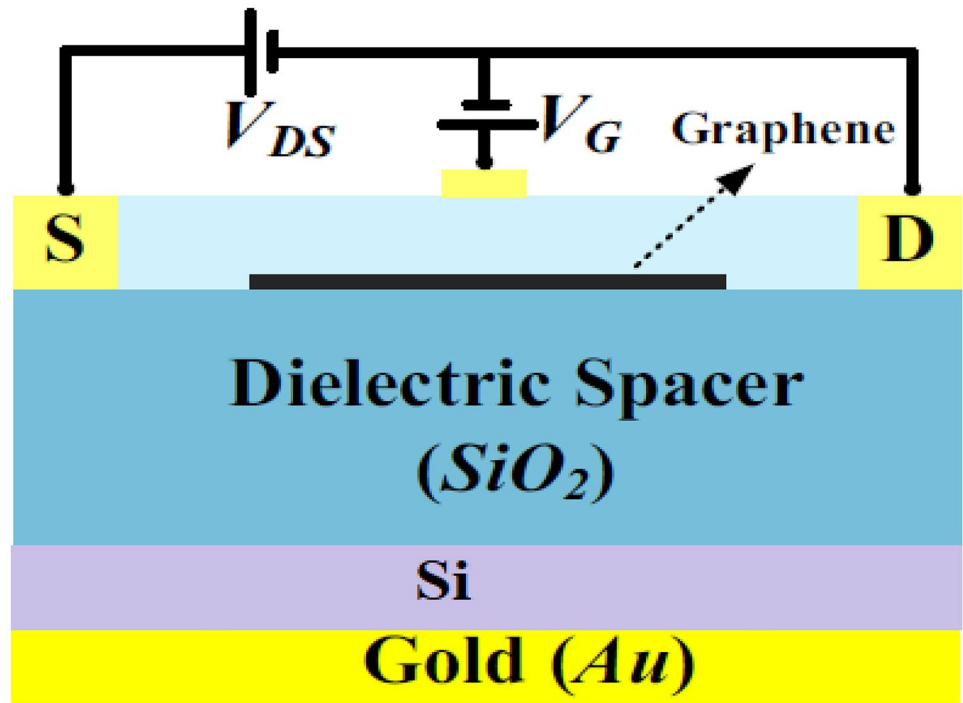


Fig. 2 Schematic of an absorber with a drain-source voltage V_{DS} and an external gate voltage V_G [22]

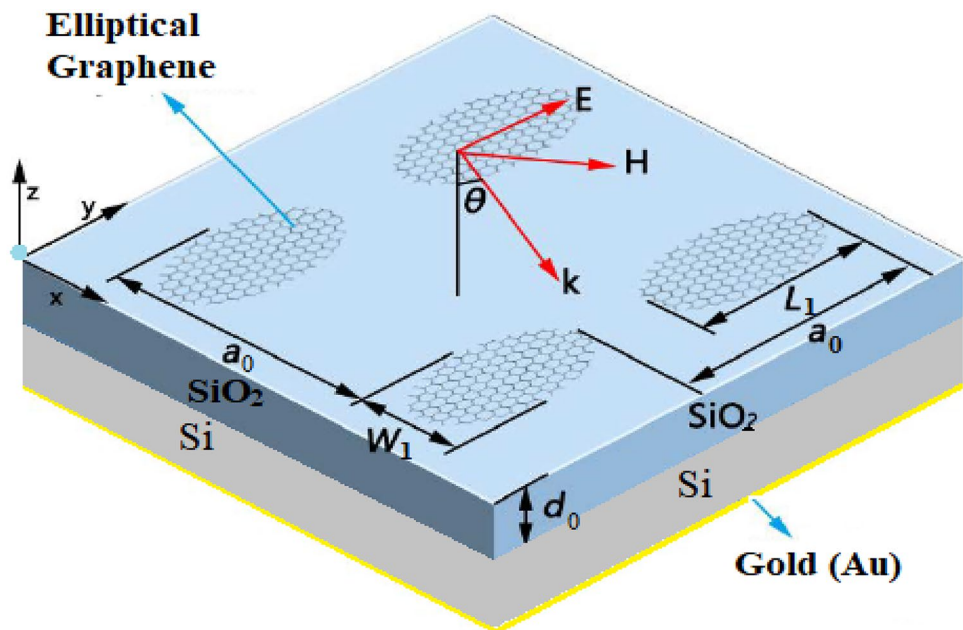


to reconstruct single crystalline surfaces. This process yielded a partially orientated polycrystalline gold surface with a roughness of less than a few nanometers. In dielectric insulating substrates, a transfer printing process may transfer graphene on gold foil. A silicon wafer coated in SiO₂ is then covered with a 100 nm thick graphene layer over PDMS [21].

A thin layer of Si is used to completely cover the graphene layer's surface is the primary approach for regularly

adjusting Fermi value of graphene [22]. An external DC bias (V_{DS}) can be used to modify the surface conductivity continually. The Fermi level can be changed by shifting resonance frequency over a wide spectral range. A thin layer of Si, which completely covers the graphene layer's surface, is one of the primary techniques for dynamically adjusting the graphene's Fermi level, as shown in Fig. 2 [22]. This material affects the absorption spectrum because of Si, transparency,

Fig. 3 Geometrical representation of elliptical graphene array



and low absorption coefficient. The proposed elliptical graphene array geometric structure diagram is shown in Fig. 3.

Graphene is arranged in an elliptical array throughout the structure. With a thickness (d_0), major axis (L_1), and short axis (W_1), graphene has been followed to a silica (SiO_2) substrate. The structural cell has a period a_0 along the Y and X axes. θ represents the plane-to-air incidence angle. It has a silicon bottom. Silicon has a refractive index of $n_{si}=1.5$, and silicon dioxide has a relative permittivity of $\epsilon_d=3.9$ [23, 24]. For the X, Y, and Z axis, the symmetric, anti-symmetric as well as PML boundary conditions were applied. The X, Y, and Z axes have 10 nm and 0.5 nm mesh precision, respectively. A plane light that moves down the negative Z-axis and is polarized along the X-axis by electric field E illuminates the entire structure. The electric field detector has been placed in the graphene layer. However, it is more significant than the graphene layer boundary. Graphene's surface conductivity closely resembles the Drude-like model [25].

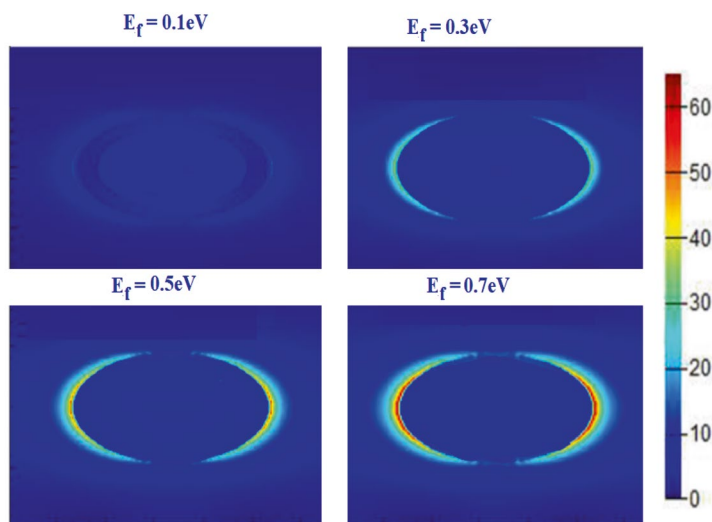
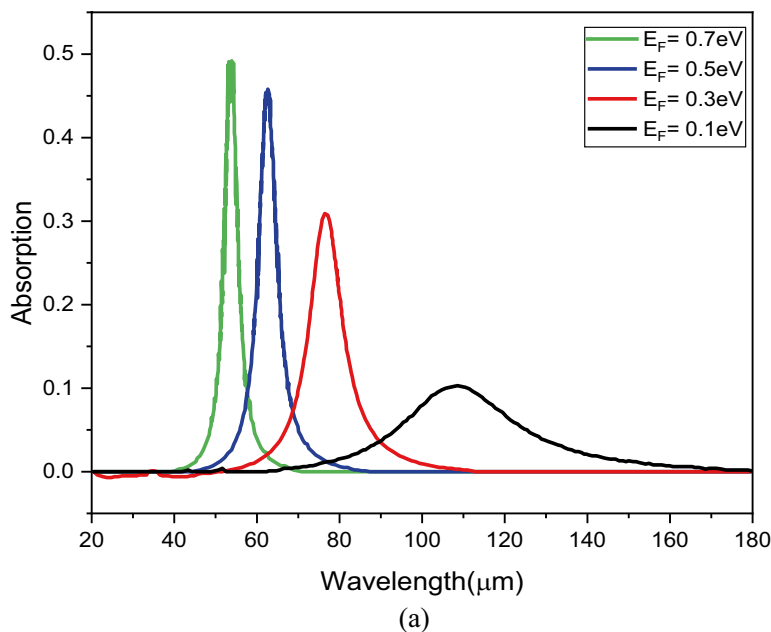
Graphene's surface conductivity closely resembles the Drude-like model [25].

$$\sigma(\omega) = \frac{e^2 \mu_c}{\pi h^{-2}} \frac{i}{\omega + \frac{i}{\tau}} \tag{1}$$

where e and h denote the electron charge and reduced Plank's constant [26]. The photon frequency (f), relaxation time (τ), and chemical potential (μ_c) are the factors that affect Eq. (1).

In this work, relaxation time and chemical potential were initially set to $\tau=0.5$ ps and $\mu_c=0.2$ eV. The entire system's

Fig. 4 **a** The absorption spectra at the Fermi level (E_F) between 0.1 and 0.7 eV. **b** The distribution for the equivalent electric field intensity based on various Fermi levels on the resonant wavelengths



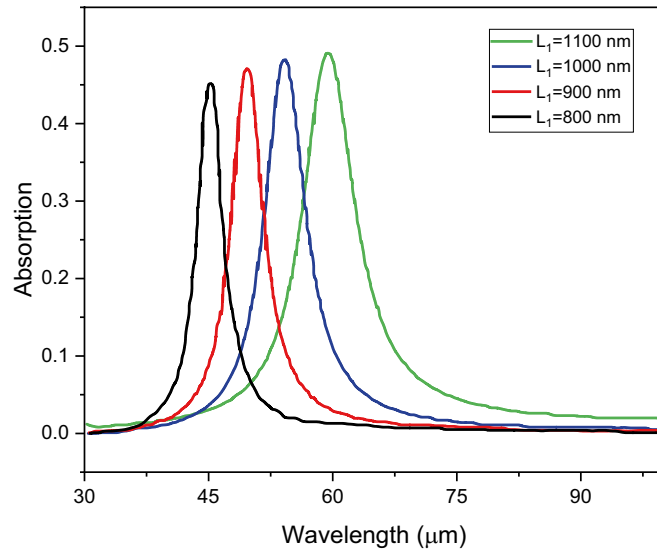
spectra are determined using finite-difference time-domain approach. For the x and y directions, we carried out symmetric and antisymmetric boundary conditions. Regarding incident propagation across the z direction, exactly matching layers are used. To determine transmission, reflection, and absorption, we define S-parameters for the simulation, which are represented by [26]:

$$T(\omega) = |S_{21}(\omega)|^2 \tag{2}$$

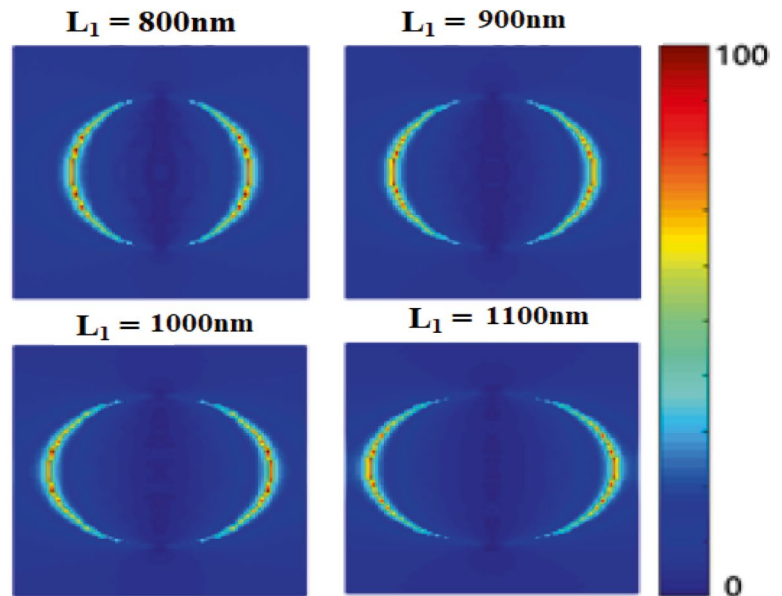
$$R(\omega) = |S_{11}(\omega)|^2 \tag{3}$$

$$A(\omega) = 1 - T(\omega) - R(\omega) \tag{4}$$

Fig. 5 a The long axis absorption spectra with various lengths. **b** Electric field distributions at absorption peaks of $L_1 = 800$ nm, 900 nm, 1000 nm, and 1100 nm



(a)



(b)

Results and Discussions

When a material’s structure remains unchanged, like graphene, it is capable of being dynamically adjusted. By altering Fermi level (E_F), graphene’s dynamic tunability is made possible. Doping or applying voltage can modify E_F dynamically [27].

The relationship between E_F and applied voltage (V_b) is stated as [27]:

$$|E_F| = \hbar v_F (\pi N)^{1/2} = (\pi \epsilon_o \epsilon_r |V_b| d_1)^{1/2} \alpha V_b^{1/2} \quad (5)$$

where ϵ_r , N , and v_F are relative permittivity of dielectric layer, total carrier density, and Fermi velocity.

The E_F will arrive at a specific value while providing a specific applied voltage. We have changed E_F values in the intervals of 0.2 eV, varies from 0.1 to 0.7 eV, and then analyzed in the absorption spectra is shown in Fig. 4a.

The maximum absorption increases approximately five times, between 10.3 and 49.6%, for 0.1 to 0.7 eV, and the resonant wavelength shifts to the blue, from 108.02 to 53.91 μm , with the absorption spectrum. Higher E_F results in higher numbers of N , which contribute to higher plasmonic oscillation, which results in higher maximum absorption [27]. The improvement results from the graphene surface plasmon resonance steadily rising as E_F increases. Thus, the localized electric field gradually gets stronger, and this stronger localized electric field has the potential to result in higher absorption. Because λ and ω are inversely related, and the corresponding absorption peak’s resonant wavelength (λ) drops as E_F increases, as shown in Fig. 4a. Consequently, ω steadily rises as λ decreases. The distribution of electric field for maximum absorption with resonant wavelengths for various E_F is shown in Fig. 4b. The

Fig. 6 a Absorption spectra for various incident angles (θ). **b** The electric field distributions for 0° , 30° , and 60° at the absorption peak

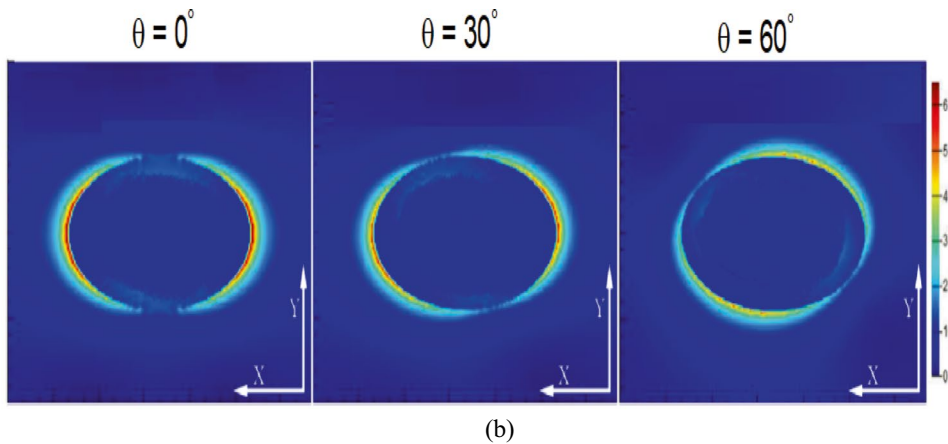
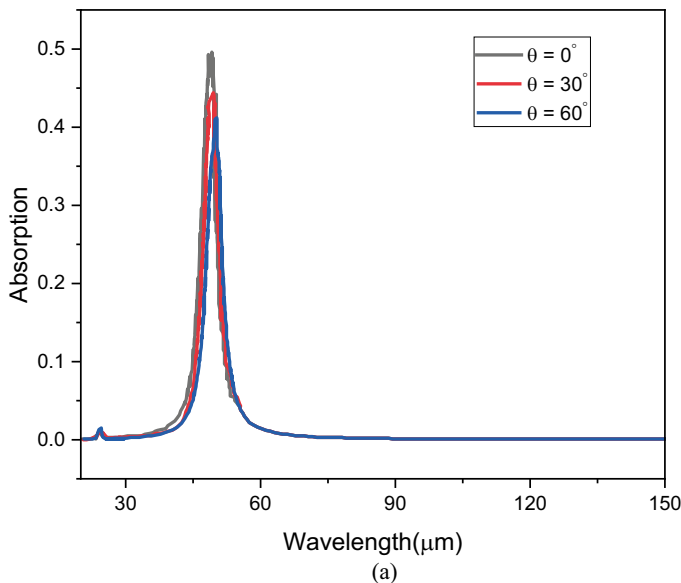
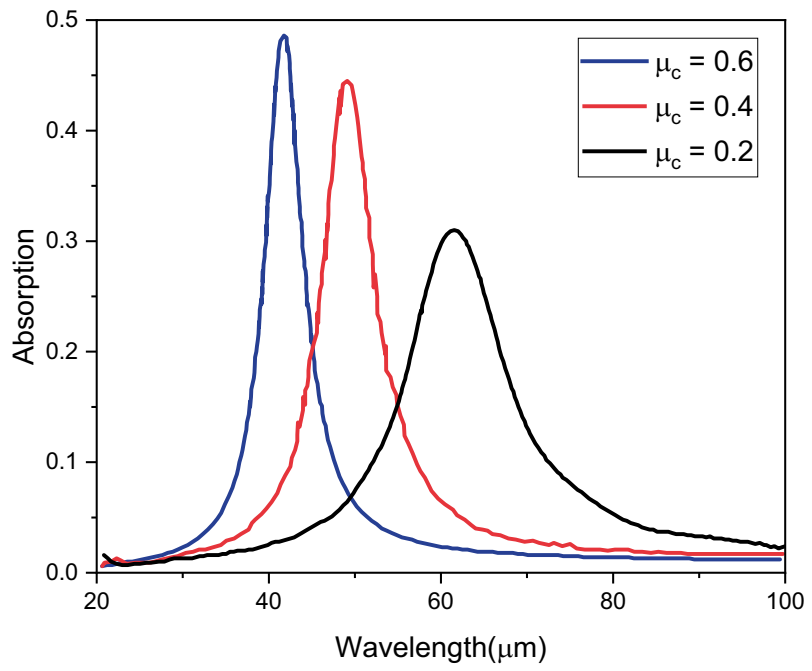
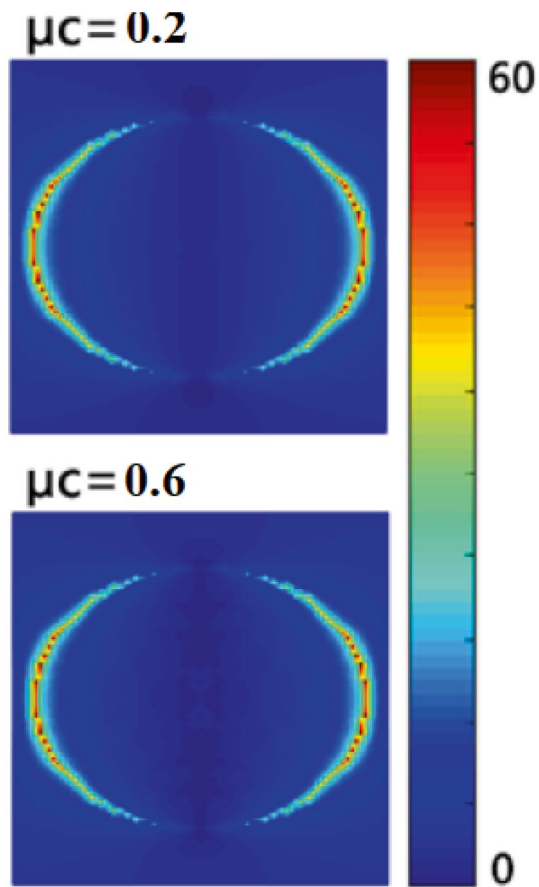


Fig. 7 a The absorption spectra for various chemical potentials (μ_c). **b** The distributions of the electric field at the absorption peak for $\mu_c=0.2$ and 0.4 eV



(a)



(b)

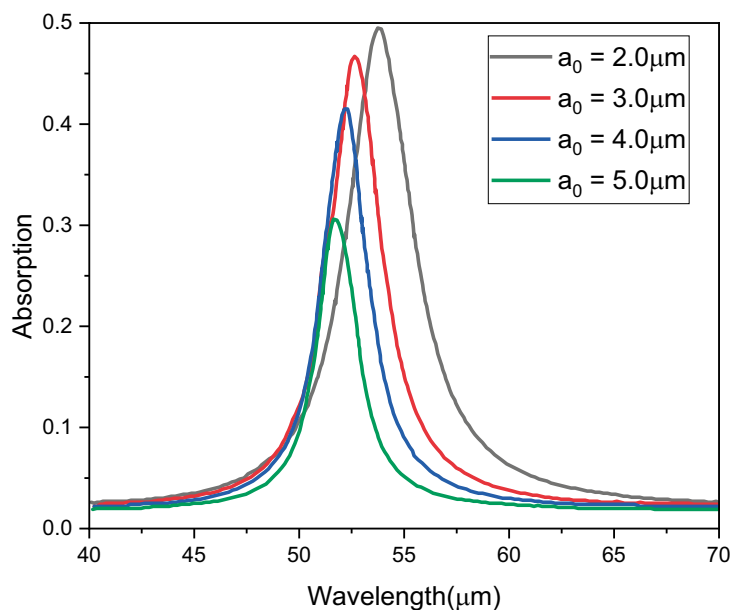
improvement occurs by the surface plasmon resonance, which rises progressively as E_F rises. The local electric field steadily increases with E_F increases, which can result in increased absorption.

The result for limiting the short axis at 800 nm in Fig. 5a demonstrates in which long axis expands, wave peak increases steadily and advances in the direction of the long wave. The resonance wavelength shifts from around 45 to 59 μm , and the peak value increases from approximately 42 to 46%. It was easy to realize that the SPR of graphene

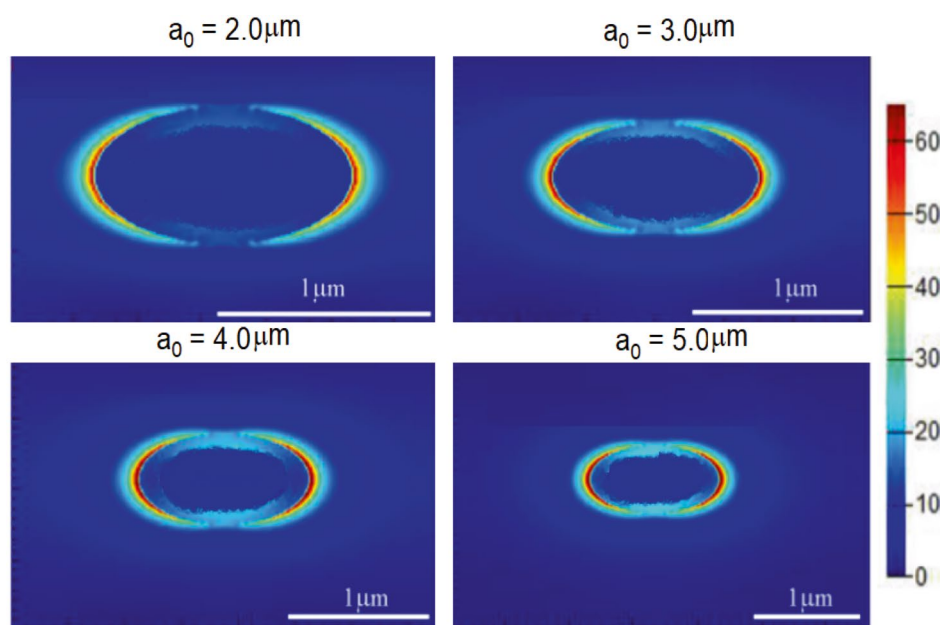
should be relevant for improved absorption. To further understand the causes of the absorption enhancement, Fig. 5b displays the electric field along a long axis of different lengths [26].

Due to the narrowing distance among subsequent elliptical arrays, graphene arrays are correlated as the long axis expands. The absorption peak is enhanced, and the red-shift is caused by increased coupling. Figure 6a shows the absorption spectra for various incidence angles. A change in incidence angle does not impact the resonance wavelength.

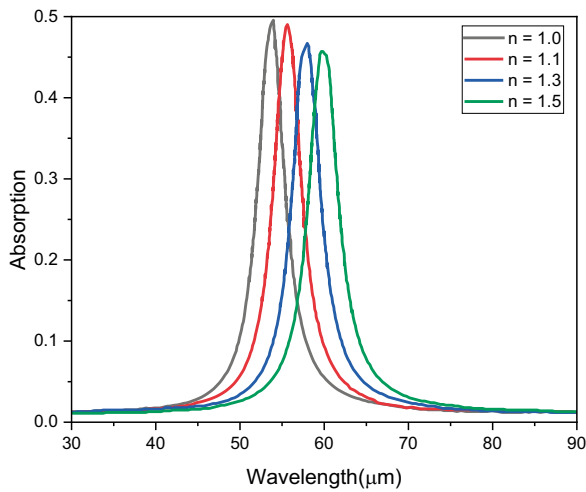
Fig. 8 **a** The simulated absorption spectra with various periods (a_0). **b** The electric field distributions of the absorption peak across various periods $a_0 = 2.0 \mu\text{m}$, $3.0 \mu\text{m}$, $4.0 \mu\text{m}$, $5.0 \mu\text{m}$



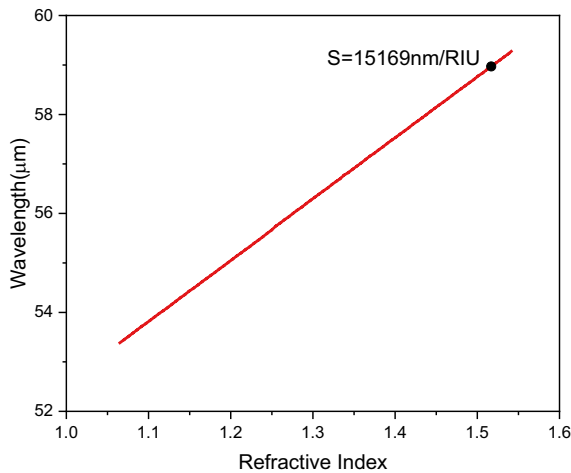
(a)



(b)



(a)



(b)

Fig. 9 **a** The absorption spectra with various refractive index (n). **b** The maximum absorption (black spot) with resonance wavelength

The resonant wavelength’s absorption peak is more sensitive to changes in incidence angle.

As the electric field intensity steadily decreases, electric field distribution goes slowly from the Y-axis to the X-axis position. Figure 6b shows the distribution of the electric field intensity at the resonant wavelength. A reduction in the electric field strength causes reduced absorption. The optical characteristics of graphene have greater impact on the chemical potential μ_c [27]. Figure 7a depicts an absorption spectra under normal incidence with several values of μ_c at $L_1=900$ nm, $a_0=2500$ nm, $d_0=300$ nm, and $W_1=750$ nm. According to the simulation results, graphene’s chemical potential causes the spectrum with blue shift to increase and their resonance wavelength to decrease. Therefore, its absorption rate will increase.

As graphene’s chemical potential increases, the wavelength of plasmons, including those related to graphene, will expand. The graphene surface’s conductivity will also increase when the chemical potential increases. As a result, light absorption is improved [26]. Consequently, the graphene layer absorbs light more and more as graphene’s chemical potential increases. The electric field distributions near the absorption peak of $\mu_c=0.2$ eV and $\mu_c=0.4$ eV are shown in Fig. 7b. The surface plasmon resonance of graphene is enhanced by its increased chemical potential. By strengthening the local electric field, absorption increases. As a result, graphene can be controlled chemically to achieve absorption control.

The effect of various periods (a_0) for absorption characteristics has been shown in Fig. 8a. The maximum absorption falls as period (a_0) increases; therefore, the resonance wavelength changes to the blue. When $a_0=2.0$ μm , the maximum absorption is 49.6%. The resonance wavelength shifts to the blue with increasing period (a_0). This is because a_0 is the determining factor of resonance wavelength when the structure and the plasmonic wave period match each other [28].

Figure 8b shows the electric field distribution with resonance wavelengths of maximum absorption with different periods (a_0). As the period increases, the edge-focused electric field intensity becomes stronger. However, when a_0 increases, the absorption gradually decreases as the graphene filling factor reduces, as well as the electric field strength impact over the absorption gradually decreases [27].

The maximum absorption decreases gradually as n increases, depicted in Fig. 9a, which leads to the resonant wavelength moving to the right and the maximum absorption changing from 49.6% at 53.96 μm to 45.7% at 59.83 μm . Figure of merit and sensitivity are essential parameters for measuring sensors. Sensitivity can be used to compute using [27]:

$$S = \frac{\Delta\lambda}{\Delta n} \tag{6}$$

FOM can be obtained by [27]:

$$FOM = \frac{S}{FWHM} \tag{7}$$

The changes in the resonant wavelength (λ) and refractive index (n) are represented by $\Delta\lambda$ and Δn , respectively. The relation that exists between refractive index and resonant wavelength is shown in Fig. 9b, where the slope line represents the sensor’s sensitivity. We determine $FOM=3.2$ and S is approximately 15,169 nm/RIU based on the relationship between FOM and sensitivity. Table 1 compares our sensitivity results with existing absorbers.

It is evident from the table that the proposed elliptical array structure has better sensing capabilities, providing an excellent reference for future studies on graphene

Table 1 Comparison of the sensitivity with several absorbers

Existing work	Proposed work	Qi et al. [27]	Li et al. [23]	Cheng et al. [2]	Li et al. [20]	Huang et al. [4]
Sensitivity ($\mu\text{m}/\text{RIU}$)	15.16	14.11	9.59	1.445	2.4	11.5

refractive index sensors. Hence, our proposed metamaterial absorber has been employed as sensor detector for monitoring changes in the environment.

Conclusion

This research article investigates the elliptical graphene metamaterial used for tunable absorption enhancement. The incidence angle, Fermi level, geometrical structure, and period have been tuned to attain the maximum absorption. The absorption rate of graphene will be increased by lengthening the ellipse's major axis, raising X polarization of the incidence angle of with specific range and improving graphene's chemical potential. It has been found that an apparent absorption peak with a maximum absorption of 49.6% occurs at 55.12 μm . The FOM and S for the refractive index sensor have the values of 3.2 and 15,169 nm/RIU, respectively. Therefore, the sensor has a strong relationship with n . An increase in the thickness of SiO_2 on the gold substrate affects the elliptical array graphene structure, which increases the absorption rate to 49.6%. Hence, the proposed elliptical array graphene structure has the potential to be applied to biosensors, environmental monitors, and graphene-based optoelectronic devices. Due to its sensing properties, the metamaterial absorber can also be used in THz smart sensing, photovoltaic devices, and clocking.

Acknowledgements The authors would like to express gratitude to Sri Eshwar College of Engineering, Karunya Institute of Technology and Sciences, Department of Technical Education Uttar Pradesh, India. The authors would also like to thank to Vice Chancellor, Dr. A.P.J. Abdul Kalam Technical University, and Uttar Pradesh, India.

Author Contribution SD and KM carried out the experiment and wrote manuscripts. BKP and DP conceived and planned the experiments, validate the outcome, and wrote manuscripts.

Data Availability The data presented in this study are available in the article.

Code Availability Not applicable.

Declarations

Ethics Approval Not applicable (as the results of studies does not involve any human or animal).

Consent to Participate Not applicable (as the results of studies does not involve any human or animal).

Consent for Publication Not applicable (as the results of studies does not involve any human or animal).

Conflict of Interest The authors declare that they have no known financial interest or personal relationships that could have appeared to influence the work reported in this paper.

References

- Bailey J, Yu X, Wen Y, Ma W, Matmon G (2015) Broadband terahertz metamaterial absorber based on asymmetric resonators with perfect absorption. *IEEE Trans Terahertz Sci Technol* 5(3):406–411. <https://doi.org/10.1109/tthz.2015.2401392>
- Cheng Y, Gong R, Wu L, Wu C, Mao XS (2016) Infrared non-planar plasmonic perfect absorber for enhanced sensitive refractive index sensing. *Opt Mater* 53:195–200. <https://doi.org/10.1016/j.optmat.2016.01.053>
- Nickpay MR, Shahzadi A, Danaie M (2021) A wideband and polarization-insensitive graphene-based metamaterial absorber. *Superlattices Microstruct* 150:106786. <https://doi.org/10.1016/j.spmi.2020.106786>
- Huang J, Yi Y, Niu G, Yi Z, Zhou Z, Chen X, Ye X, Yi Y, Tang Y, Duan T (2019) High sensitivity refractive index sensing with good angle and polarization tolerance using elliptical nanodisk graphene metamaterials. *Phys Scr* 94(8):085805. <https://doi.org/10.1088/1402-4896/ab185f>
- Zhang X, Yan C, Gong H, Qi Y, Zhou P, Hu B (2018) Refractive index sensor based on Fano resonances in plasmonic waveguide with dual side-coupled ring resonators. *Photonic Sensors* 8(4):367–374. <https://doi.org/10.1007/s13320-018-0509-6>
- Qin F, Yi Y, Duan T, Chen X, Yao W, Yi Z, Wu P, Li G, Yang H, Chen Z (2020) A tunable triple-band near-infrared metamaterial absorber based on Au nano-cuboids array. *Nanomaterials* 10(2):207. <https://doi.org/10.3390/nano10020207>
- Hu H, Huang X, Zhao Y, Zhang X, Wang Y, Qi B (2022) A graphene-based THz metasurface sensor with air-spaced structure. *Front Phys* 10. <https://doi.org/10.3389/fphy.2022.990126>
- Neebha TM, Dhanasekar S, Bruntha PM, Andrushia AD, Manjith R, Durga S (2021) Analysis of multilayered antennas with slotted ground for bandwidth enhancement. 2021 7th international conference on advanced computing and communication systems (ICACCS). <https://doi.org/10.1109/icaccs51430.2021.9441806>
- Dhanasekar S (2020) An ultra-low-power static random-access memory cell using tunneling field effect transistor. *Int J Eng* 33(11). <https://doi.org/10.5829/ije.2020.33.11b.13>
- Bruntha PM, Dhanasekar S, Pandey BK, Neebha TM, Pandey D, Sagayam KM (2022) Application of switching median filter with L2 norm-based auto-tuning function for removing random valued impulse noise. *Aerospace Systems* 6(1):53–59. <https://doi.org/10.1007/s42401-022-00160-y>
- Xiao B, Xiao L, Cai W, Wang Y (2022) Design and prediction of PIT devices through deep learning. *Opt Express* 30(9):14985. <https://doi.org/10.1364/oe.449465>
- Neebha TM, Andrushia AD, Dhanasekar SP, Varshney A, Manjith R (2023) On the design of miniaturized C-shaped antenna based on artificial transmission line loading technique. *J Electromagn*

- Waves Appl 37(6):814–826. <https://doi.org/10.1080/09205071.2023.2211282>
13. Chen J, Yang L, Zhang Y, Wang X, Ye X, Tang F (2020) Substrates for surface-enhanced Raman spectroscopy based on TiN plasmonic antennas and waveguide platforms. *Results Phys* 16:102867. <https://doi.org/10.1016/j.rinp.2019.102867>
 14. Jubair Ahmed L, Martin Sagayam K, Anish Fathima B, Dhanasekar S (2022) Modeling of fuzzy logic-based classification system using the gravitational search algorithm. *Multimedia technologies in the internet of things environment* 3:79–94. https://doi.org/10.1007/978-981-19-0924-5_5
 15. Alaae R, Lederer F, Farhat M, Rockstuhl C (2012) A perfect absorber made of a graphene micro-ribbon metamaterial. *Opt Express* 20(27):28017. <https://doi.org/10.1364/oe.20.028017>
 16. Zhang Y, Jiang T, Zhao J, Zhu B, Feng Y (2014) Graphene based tunable metamaterial absorber and polarization modulation in terahertz frequency. *Opt Express* 22(19):22743. <https://doi.org/10.1364/oe.22.022743>
 17. Xiao S, Yan X, Liu Y, Han X, Xu C, Wang T (2016) Tunable light trapping and absorption enhancement with graphene ring arrays. *Phys Chem Chem Phys* 18(38):26661–26669. <https://doi.org/10.1039/c6cp03731c>
 18. Esfandiari M, Szczepanski S, Jarchi S, Noori Mahtaj H, Alibakhshikenari L, M., Reisenfeld, S., & Koziel, S. (2022) Recent and emerging applications of graphene-based metamaterials in electromagnetics. *Mater Des* 221:110920. <https://doi.org/10.1016/j.matdes.2022.110920>
 19. Fang Z, Schlather AE, Halas NJ, Liu Z, García de Abajo FJ, Ajayan PM, Nordlander P, Zhu X, Wang Y (2013) Active tunable absorption enhancement with graphene nanodisk arrays. *Nano Lett* 14(1):299–304. <https://doi.org/10.1021/nl404042h>
 20. Li R, Ye H, Liu Y, Yu Z, Yu L, Wu D (2017) Infrared plasmonic refractive index sensor with ultra-high figure of merit based on the optimized all-metal grating. *Nanoscale Res Lett* 12(1). <https://doi.org/10.1186/s11671-016-1773-2>
 21. Pince E, Oznuluer T, Polat EO, Kocabas C, Salihoglu O, Balci O (2011) Synthesis of graphene on gold. *Appl Phys Lett* 98(18). <https://doi.org/10.1063/1.3584006>
 22. Nickpay M-R, Shahzadi A, Danaie M (2022) Graphene-based metamaterial absorber for refractive index sensing applications in terahertz band. *Diam Relat Mater* 130:109539. <https://doi.org/10.1016/j.diamond.2022.109539>
 23. Li K, Song G, Zhang Z, Xu Y, Song J, Ma X (2014) Sensitive refractive index sensing with tunable sensing range and good operation angle-polarization-tolerance using graphene concentric ring arrays. *J Phys D Appl Phys* 47(40):405101. <https://doi.org/10.1088/0022-3727/47/40/405101>
 24. Cen C, Xiao S, Zhang Y, Chen X, Zhou Z, Tang Y, Ye X, Liu L (2019) Tunable absorption enhancement in periodic elliptical hollow graphene arrays. *Opt Mater Express* 9(2):706. <https://doi.org/10.1364/ome.9.000706>
 25. Cen C, Yi Y, Chen Z, Chen X, Yi Z, Jiang L, Li G, Wu P, Xu D (2020) High quality factor, high sensitivity metamaterial graphene—perfect absorber based on critical coupling theory and impedance matching. *Nanomaterials* 10(1):95. <https://doi.org/10.3390/nano10010095>
 26. Chen J, Yi C, X., Yi, Z., Xu, X., Zhou, Z., Xiao, S., Ye, X., Shi, P., & Y., Zeng, Y. (2018) Plasmonic absorption enhancement in elliptical graphene arrays. *Nanomaterials* 8(3):175. <https://doi.org/10.3390/nano8030175>
 27. Qi Y, Wang X, Zhang T, Wang L, Zhang Y, Deng X, Zhang B, Bai Y, Liu C (2020) A tunable terahertz metamaterial absorber composed of elliptical ring graphene arrays with refractive index sensing application. *Results Phys* 16:103012. <https://doi.org/10.1016/j.rinp.2020.103012>
 28. Fang Z, Halas NJ, Wang Y, Liu Z, Ajayan PM, Schlather AE, Nordlander P, Zhu X, García de Abajo FJ (2013) Active tunable absorption enhancement with graphene nanodisk arrays. *Nano Lett* 14(1):299–304. <https://doi.org/10.1021/nl404042h>

Publisher's Note Springer Nature remains neutral with regard to jurisdictional claims in published maps and institutional affiliations.

Springer Nature or its licensor (e.g. a society or other partner) holds exclusive rights to this article under a publishing agreement with the author(s) or other rightsholder(s); author self-archiving of the accepted manuscript version of this article is solely governed by the terms of such publishing agreement and applicable law.